RSC Advances

ROYAL SOCIETY OF CHEMISTRY

www.rsc.org/advances

Journal Name ARTICLE

Boron nitride nanosheets with controlled size and thickness for enhancing mechanical properties and atomic oxygen erosion resistance

Lei Liu,[ac] Zhigang Shen,*[ab] Yiting Zheng,[c] Min Yi,[ab] Xiaojing Zhang[a] and Shulin Ma[a]

The comprehensive effects of the dimension and the thickness of boron nitride nanosheets (BNNSs) on the composite properties are evaluated in this study. BNNSs were directly prepared in cellulose acetate (CA)-acetone solution and separated into different size ranges by multi-step centrifugation, while composite films were then fabricated by employing as-prepared nanosheets as fillers and CA, a biodegradable polymer, as the matrix. Break elongation was significantly increased by filling large BNNSs due to the reduction of bubble defects and the slowdown of the crack propagation. Importantly, "zipper crack" consists of two ordered and meshing protruding teeth, contributing to high energy absorption and fracture toughness. Large surface area in one plane and high stability of BNNSs can effectively protect the polymer matrix from atomic oxygen (AO) erosion. Furthermore, the embedment of BNNSs with high aspect ratio can achieve significant enhancement of mechanical properties and AO erosion resistance. All results indicate that boron nitride sheet is promising nanofiller for polymeric composites and, more importantly, high aspect ratio is the critical factor for achieving the desired improvement.

Introduction

Two dimensional (2D) nanosheets have great potential for various applications due to their extraordinary physical and chemical properties.[1-3] Graphene, a 2D honeycomb lattice carbon material, exhibits excellent electrical and mechanical properties, providing new strategies for developing electronic devices and high-performance composites.[4-7] In addition, large quantities of novel 2D ordered crystal materials also aroused great interest of the researcher, especially hexagonal Boron nitride (h-BN) and molybdenum disulfide (MoS_2).[2, 3, 8-13] h-BN is a layered structural material which as a set of BNNSs stacked orderly. Similar to graphene, BNNSs also have many outstanding properties, such as thermoconductive, lubrication, corrosion resistance and mechanical strength.[14-18] The 2D elastic modulus of boron nitride nanosheet with a thickness of 1-2 nm was measured in the range of 200-500 N m^{-1}, suggesting that it is an ideal nanofiller to reinforce polymer.[2]

2D nanosheets can be advantageously combined with various polymers and afford distinguishing characteristics to composites. Homogeneous dispersing of nanofillers is important in terms of efficient stress transfer between different components. At present the agglomeration and restacking of nanosheets are still the main challenges on account of their high surface energy and low solubility in most solvents. Surface modification is a common method to tackle these problems, but it tends to destroy the structure or reduce the properties of materials.[19, 20] But CA molecules can also reduce agglomeration of nanosheets by absorbing at BNNSs surfaces, resulting from the steric stabilization mechanism.[21] As a major component, the incorporation of polymer molecules can not only significantly enhance the dispersion stability, but also make an ideal starting point for the composite formation.[20] The effects of thickness and size of nanosheets are usually ignored in most researches. Coleman et al. have found that the mean sizes of graphene and MoS_2 nanosheets have obvious effects on the mechanical properties of composite film.[22, 23] Actually, 2D sheets generally thicken with an increase in lateral dimensions and both of thickness and lateral size have significant influence on the composite properties. So we employed the aspect ratio (length/thickness) to roughly represent this integrative change. CA is a biodegradable polymer and few reports mentioned that it was composited with 2D nanosheets. Consequently, we employed multi-step centrifugation to obtain relatively uniform BNNSs and then prepared composite films by using CA as polymer matrix in this study.

AO erosion resistance is an important property for spacecraft materials in low earth orbit, which can prevent them from being oxidized and eroded by high-energy AO. Polymers are widely applied in the spacecraft as structural and thermal protection materials, but they are particularly vulnerable to AO.[24] Coatings of inorganic oxide have been used to provide protection from atomic oxygen, but they are brittle, heavy, expensive and have weak interaction with polymer.[25] Meanwhile, it is difficult for zero-dimension and one-dimension nanofillers to form a dense protective covering to defend AO erosion, but 2D nanosheets can provide large enough protecting surface area in one plane. h-BN has been proved to high stability for chemical and heat corrosion.[26-29] Importantly, the gradual substitution of oxygen atoms for nitrogen atoms and vacancies can be induced by AO, but the chemical bonds between oxygen atoms and nanosheets are too strong to be destroyed by subsequent erosion[30, 31] Additionally, the gas barrier of BNNSs can prevent atomic oxygen migration and penetration.[32] Therefore, BNNSs are considered as prefect and lightweight nanofillers to enhance AO erosion resistance of space materials.

Here, we demonstrated that h-BN was effectively exfoliated to form a stabilized dispersion by adding CA as the stabilizer. The size and thickness of BNNSs were controlled in certain range by multi-step centrifugation and their influences on the composite properties were discussed. Importantly, it is noteworthy that the reduction of bubble defects and the emergence of "zipper cracks" by embedding BNNSs are first reported in this article. High aspect ratio of nanosheets is more advantageous for improving properties of composite materials. Moreover, using BNNSs with outstanding stability as fillers can obviously improve the AO erosion resistance of polymeric

composites. It is anticipated that the reinforcing mechanism of BNNS in mechanical properties and AO erosion resistance could broaden the applications in various important fields.

Experimental

Exfoliation of h-BN in CA solution: h-BN was purchased from Alfa Aesar (Product Number: 011078). CA was obtained from Sinopharm Chemical Reagent Co., LTD (acetyl value: 54.5–56%). CA powder was dispersed in the acetone and then subjected to magnetic stirring under the sealed condition for 4 h. CA concentrations were controlled from 1 to 9 mg ml^{-1} at 1 mg ml^{-1} interval. h-BN powder (60 mg) was added in 30 ml pure acetone and CA-acetone solutions with different CA contents. These mixtures were shaken well and treated by sonication for 4 h(KQ2200DE, Kunshan, China). After that, all dispersions were placed for two weeks to analyze the stability of BNNSs dispersions.

Preparation of BNNSs/CA composite films*:* h-BN powder (8 g) was dispersed in 400 ml CA-acetone solution (3mg ml^{-1}) and then was sonicated for 100 h. BNNSs dispersions were separated by multi-step centrifugation. Firstly, the dispersion was centrifuged at a higher rate of 2000 rpm (the centrifugal acceleration is about 1015 g), separating the small BNNSs in the supernatant from the larger nanosheets in the sediment. Supernatant was removed from the dispersion by pipette. Secondly, the sedimentation was washed using acetone and then dispersed in 200 ml CA-acetone solution again by sonication for 2h. By repeating the above steps, relatively large BNNSs were centrifuged at low speed: 1500 rpm (about 571 g), 1000 (about 253 g) and 500 rpm (about 63 g). All cases were carried out using an LD4-40 industrial centrifugal machine (Jingli, China.) for 60 min. Supernatants were diluted or concentrated to achieve the proper concentration of BNNSs. CA concentration of all dispersions need to reach 10mg ml^{-1} by adding CA powder. The mixtures were then subjected to the magnetic stirring for 4 h and placed for 10 h to reduce bubble. The above dispersions were flattened on the glass plate by a glass rod, and then left to dry at room temperature for 2h. The BNNSs contents of composite films were controlled to be 0.25, 0.5, 1, 2, 4 wt%, respectively. For comparison, pure CA film was also prepared.

Atomic oxygen effects simulation experiment: AO exposure experiments were performed in the ground-based AO effects simulation facility under 0.15 Pa, the filament discharge voltage is 120 V and the discharge current is 100 mA.[33] After AO exposure, all samples were weighed and mass loss per unit area could be calculated. The atomic oxygen flux was calculated using the mass loss of Kapton in the atomic oxygen exposure experiments. [33] The calculation formula is $Ft = \Delta M/(\rho A E_y)$ in which F is the effective flow rate of atomic oxygen onto the sample surface and ΔM, ρ, A, t, E_y are mass loss, density, surface area, exposure time, and erosion yield, respectively. Ft is the accumulative atomic oxygen flux exerting on the sample surface. In this study, the accumulative atomic oxygen was about 1.6×10^{20} atoms cm^{-2}.

Sample preparation and Characterizations: To diminish the effects of CA on the morphology of BNNSs, the filter cakes were washed four times with acetone. BNNSs for scanning electron microscopy (SEM) were prepared by vacuum filtering the dispersions onto porous membranes. The fracture surfaces were tore after liquid nitrogen freezing and coated with platinum. The samples for atomic force microscopy (AFM) and transmission electron microscopy (TEM) were prepared by dropping the dispersion onto freshly cleaved mica surfaces and holey carbon grids, respectively. SEM images were obtained by JSM-6010 (JEOL, Japan). Atomic force microscopy was performed in Multimode 8 (Bruke, USA) which was operated in ScanAsyst Air mode. JEM-2100 (JEOL, Japan) was used to characterize the morphology of BNNSs. TGA analysis was performed on SDTA851 (Mettler Toledo, USA) at 10°C min^{-1} in an aluminum crucible under N_2. UV-Vis absorption spectroscopy was performed with TU1901 (Purkinje, China) and the concentration was calculated from the Lambert – Beer law.[34] Mechanical tests were measured by an electronic stretching machine (Instron 5565, Instron Engineering, American) at a strain rate of 2 mm min-1 with a gauge length of 30 mm. The samples were cut into strips of 15 mm wide and 60 mm long. Reported data on Young's modulus, tensile strength, and breaking elongation at rupture are the averages of 4 strips of the same sample. All the failure occurred at the middle region of the testing strips.

Results and Discussion

As seen in Fig. 1a, production of BNNSs/CA composite films contains serveral steps, including ultrasonic exfoliation, centrifugal separation, preparation of solutions and composite films (see experimental procedure). As shown in Fig. 1b, the addition of CA can obviously improve the stability of BNNSs dispersions. A slow sedimentation was observed in all samples containing CA and this tendency became noticeable when the concentration was beyond 2mg ml^{-1}. However, we noted that the partial sedimentation occurred in solutions with high CA contents because of the inadequate exfoliation in high viscosity solution. Hence 3 mg ml^{-1} is considered to be the appropriate concentration for the production and preservation of BNNSs dispersions.

As seen in Fig. 1c, the transparency of smooth and uniform composite films becomes worse with increasing BNNSs content. The inset in Fig. 1c shows a smooth and flexible composite film, indicating it still retains high ductile properties of polymer. In addition, a few bubbles could be observed in pure CA film (Fig. S1, see ESI). Bubbles, pockets of air or solvent vapor, easily generated and deposited in the polymer films, which have greatly negative effect on the mechanical properties of polymers. The effects of graphene flakes on reducing bubble defects have been proved, and BNNSs also have similar effects (see ESI).[35] Small bubbles captured by BNNSs can converge to form large bubbles, and then were finally eliminated through BNNSs near the surface. Above all, the stress concentration induced by residual bubbles can be effectively transferred through nearby BNNSs owing to their high surface area and excellent elastically deformation.[2] Therefore, BNNSs can increase the degassing speed and reduce the negative effects of bubbles. In order to learn about the exfoliated h-BN particles, we investigated the micro-morphology before and after sonication. As shown in Fig.

S2, pristine h-BN particles were well exfoliated into thin sheets and the size distribution is quite broad (see ESI). More importantly, the HRTEM image and XRD pattern of BNNSs reveals high crystalline of BNNSs, indicating the hexagonal crystal structure of the BNNSs was not destructed by sonication

We further performed AFM and TEM analyses to investigate the selected nanosheets. Fig. 2a-d display typical AFM and TEM images of BNNSs separated with 500 and 2000 rpm, respectively. Obviously, high final centrifugal speed is beneficial to get small and thin sheets. As shown in Fig. 2a,c, for BNNSs obtained with 500 rpm, the mean length and width reached 4.5 μm and 3.1 μm, respectively, and the thickness increased to 3.4 nm. By comparison, the height scale of 2000 rpm sample is about 1.3 nm, which is the characteristic of fully exfoliated BNNSs, [36, 37] and they have a mean length and width of 0.6 μm and 0.8 μm, respectively (Fig. 2b,d). Moreover, the statistical data of the size and thickness determined by AFM analysis were plotted in Fig. 2e. The average thickness and size concentrated in certain small range and both decreased as the rotation rate increased, thus the aspect ratio was further used to reflect this synchronous change. Fig. 2e shows that sheets obtained at 1500 rpm have the highest aspect ratio, while sheets selected at 2000 rpm have the lowest because of their small size.

Recent researches shown that individual h-BN monolayers have relatively high bulk modulus around 160 Pa·m, as compared to 202 Pa·m of graphene.[3] As shown in Fig. 3b, the addition of BNNSs separated with 2000 rpm shows unsatisfied effects on mechanical properties of composite films, which is similar to results of the polyurethane films filled by graphene flakes.[21] Small sheets cannot provide enough contact area to transfer the stress and have limited effects on the improvement of mechanical properties.[21, 23] Above all, only BNNSs separated at 1500 rpm, which exhibit relatively larger aspect ratio than the other ones, contributed to the significant improvement of modulus and breaking elongation. However, composite films containing thick BNNSs selected with 1000 and 500 rpm showed unsatisfied modulus. As the number of layers increases, the mechanical properties of BNNSs slowly improve and yet the reinforcement effects by adding equal amounts of the nanofillers is actually reduced. Besides, low specific surface area of thick sheets and relatively weak shear strength of interlayers can further influence the modulus of composite films[38-40] To our surprise, the break strain shown a contrary tendency compared with that of modulus, which is also different from the decrease of break strain by embedding 2D nanosheets in other works.[41] For one thing the significant improvement of break elongation may be caused by efficiently reducing of bubbles through large sheets. For another, large BNNSs can provide larger contact area to effectively transfer stress and form irregular cracks to slow down the disruption of polymer molecular chains.

The fracture toughness is an important ability to resist the fracture and improve the mechanical properties.[42-44] The deflection and the slowdown of crack propagation can be observed in Fig. 3b-e. As shown in Fig. 3b, cracks are relatively straight and smooth owing to weak effects of small BNNSs on blocking and deflecting of cracks. For comparison, the barriers formed by larger BNNSs require higher strain energy to overcome, resulting in the interrupt of the continuing cracks (Fig. 3d). Moreover, Fig. 3c, e show the special "zipper cracks" which consist of two orderly rows of protruding teeth with the approximate dimension (about 3 μm, similar with sheets size). These complex and uniform cracks tremendously increased the crack length, improving the energy absorption and the fracture toughness. Formation area of "zipper cracks" is generally close to the stress concentration areas because the formation and the growth of "zipper cracks" need high enough energy (Fig. S5, see ESI). Above all, "zipper cracks" could not be observed in the 2000 rpm samples, indicating that the meshing and protruding teeth may be induced by large BNNSs with relatively uniform size. To increase the contents of 1500 rpm sheets can remarkably improve the tensile behavior of CA films: both modulus and tensile strength increased gradually (Fig. S6, see ESI). As for 2 wt% of BNNSs/CA nanocomposite films, modulus and tensile strength are 7.9 GPa and 121 MPa, corresponding to increases of 12.4 % and 14 %, respectively (relative to the pure CA film).

Fig. 4a,b further investigate the dispersing of BNNSs in the composites. As compared to the relatively smooth fractured surface of pure CA (Fig. 4c), many protruding flakes are obviously shown in the fracture surface of composite films. Moreover, the aggregation of BNNSs cannot be identified from the images, confirming that BNNSs adhered with CA molecules can be uniformly dispersed and remain stable throughout the entire producing process. However, the protruding flakes are larger and thicker than BNNSs investigated by AFM possibly due to flake surfaces might be covered with a thin layer of CA, illustrating the strong interaction between the filler and matrix. It should be noticed that almost all BNNSs are parallel to the plane of the composite films owing to the directional flow induced by the shearing force during the coating process.

The translational energy of AO collisions is about 4.5-5 eV, which is sufficient to break the polymer bond and induce oxidative decomposition.[45] As shown in Fig. 4d, e, the relatively smooth surface of pure CA sample became rough and formed the homogeneous "peaks and troughs" after AO exposure. In contrast, BNNSs were exposed on the surface because the top polymer was eroded away at the early period (Fig. 4f). However, BNNSs were not destroyed by AO and can play key role in protecting underneath CA as 2D shields. What is more, almost all BNNSs parallel arranged to the surface, achieving the maximum efficiency. The edge view shows that the diffused AO can destroy the underneath polymer through the gaps between BNNSs and form the laminated "mushrooms", hence the densification of covered BNNSs also influences the AO erosion resistance (Fig. 4g, h). As seen in Fig. 5a-d, the mean size of BNNSs exposed on the surface enlarges as decreasing the separation rates. Interestingly, the composite films containing small sheets possessed too many gaps to protect underneath polymer from the diffused AO, but the collapse of "mushrooms" can accelerate the

formation of dense protective covering. Therefore, compared with the 500 rpm and 1000 rpm composite films, higher centrifugal speed samples have better AO erosion resistance (Fig. 5e). Besides, the embedment of 1500 rpm sheet achieves the highest AO erosion resistance due to relatively high aspect ratio and fewer gaps. It should be emphasized that large BNNSs can provide larger protective area and less gaps than that of small nanosheets with the same thickness, which can provide more effective protection. Therefore the production of large and thin BNNSs will become the focus in further research.

As the filler contents increased, more BNNSs protruding the surface could rapidly improve the covering density, contributing to the reduction of the mass loss (Fig. S7a-d, see ESI). It is clear that the densification of BNNSs covering could directly influence the AO erosion resistance. Compared with low contents samples, the mass loss of 4wt % BNNSs/CA composite film significantly decreased. This demonstrated that the dense protective covering can excellently defend AO erosion and weaken the damage of AO diffusion. As seen in Figure 5e, additions of only 1, 2, and 4 wt% BNNSs can achieve 39.6, 55.9, and 61.3% decrease in mass loss, respectively. In short, these results of the mass loss and surface morphology indicated that BNNSs can substantially improve the AO erosion resistance. Based on this research, there is a potential to choose large and thin BNNSs, increase the content of BNNSs and select more stable polymer for better protective effectiveness Fig. S8 shows that the thermal stability of composite films is also slight improved by the incorporation of BNNSs.

Conclusions

This work demonstrated comprehensive effects of thickness and size on the mechanical properties and AO erosion resistance of BNNSs reinforced composite films. The stability of BNNSs dispersion can be enhanced by adding CA as the stabilizer and this strategy contributes to homogeneous dispersing of nanosheets in polymer. BNNSs with relatively broad size distributions can be separated into different size ranges by multi-step centrifugation. Too small flakes cannot provide large enough contact area with polymer matrix to effectively transfer the stress, leading to weak reinforcing effect. But lager nanosheets tend to be thicker in contrast with smaller ones. We also observe obviously improvement of the break elongation and yet low modulus by adding excessively large and thick BNNSs. The reducing of bubble defects and novel “zipper cracks” may deepen the reinforcing mechanisms of embedding 2D nanosheets. BNNSs have high specific surface area and excellent stability, making it as idea nanofiller to enhance the AO erosion resistance. And high aspect ratio and relatively less gaps between nanosheets may result in better enhancing effect. By conducting this work, we propose a novel way to prepare composite material of high performance, and hope this considerable conclusion as to comprehensive effect of the thickness and size can be used to design more composite materials.

Acknowledgements

This work was funded by Beijing Natural Science Foundation (Grant No. 2132025), the Special Funds for Co-construction Project of Beijing Municipal Commission of Education, and the Fundamental Research Funds for the Central Universities, .the Specialized Research Fund for the Doctoral Program of Higher Education (Grant No. 20131102110016)

Notes and references

[a] Beijing Key Laboratory for Powder Technology Research and Development, Beijing University of Aeronautics and Astronautics, Beijing 100191, China. E-mail: shenzhg@buaa.edu.cn;

[b] Ministry of Education Key Laboratory of Fluid Mechanics, Beijing University of Aeronautics and Astronautics, Beijing 100191, China

[c] School of Material Science and Engineering, Beijing University of Aeronautics and Astronautics, Beijing 100191, China

† Electronic Supplementary Information (ESI) available: [details of any supplementary information available should be included here]. See DOI: 10.1039/b000000x/

1. M. Cai, D. Thorpe, D. H. Adamson and H. C. Schniepp, *J. Mater. Chem.*, 2012, **22**, 24992-25002.
2. L. Song, L. Ci, H. Lu, P. B. Sorokin, C. Jin, J. Ni, A. G. Kvashnin, D. G. Kvashnin, J. Lou and B. I. Yakobson, *Nano Lett.*, 2010, **10**, 3209-3215.
3. A. Nag, K. Raidongia, K. P. Hembram, R. Datta, U. V. Waghmare and C. Rao, *ACS nano*, 2010, **4**, 1539-1544.
4. X. Zhang, B. R. S. Rajaraman, H. Liu and S. Ramakrishna, *RSC Advances*, 2014, **4**, 28987-29011.
5. Y. Su and Y. Lv, *RSC Advances*, 2014, **4**, 29324-29339.
6. G. Zhao, T. Wen, C. Chen and X. Wang, *RSC Advances*, 2012, **2**, 9286-9303.
7. X. Huang, X. Qi, F. Boey and H. Zhang, *Chem. Soc. Rev.*, 2012, **41**, 666-686.
8. G. Elumalai, H. Noguchi and K. Uosaki, *Phys. Chem. Chem. Phys.*, 2014.
9. L. Liu, T.-K. Sham and W. Han, *Phys. Chem. Chem. Phys.*, 2013, **15**, 6929-6934.
10. X. Wang, C. Zhi, L. Li, H. Zeng, C. Li, M. Mitome, D. Golberg and Y. Bando, *Adv. Mater.*, 2011, **23**, 4072-4076.

11. C. Zhi, Y. Bando, C. Tang, H. Kuwahara and D. Golberg, *Adv. Mater.*, 2009, **21**, 2889-2893.
12. B. Mortazavi and G. Cuniberti, *RSC Advances*, 2014, **4**, 19137-19143.
13. B. L. Li, H. Q. Luo, J. L. Lei and N. B. Li, *RSC Advances*, 2014, **4**, 24256-24262.
14. C. Li, Y. Bando, C. Zhi, Y. Huang and D. Golberg, *Nanotechnology*, 2009, **20**, 385707.
15. S. K. Singh, M. Neek-Amal, S. Costamagna and F. Peeters, *Phys. Rev. B*, 2013, **87**, 184106.
16. D.-H. Cho, J.-S. Kim, S.-H. Kwon, C. Lee and Y.-Z. Lee, *Wear*, 2013, **302**, 981-986.
17. Y. Lin, C. E. Bunker, K. S. Fernando and J. W. Connell, *Acs Appl. Mater. Interfaces*, 2012, **4**, 1110-1117.
18. M. A. Rafiee, T. N. Narayanan, D. P. Hashim, N. Sakhavand, R. Shahsavari, R. Vajtai and P. M. Ajayan, *Adv. Funct. Mater.*, 2013, **23**, 5624-5630.
19. S. Liu, J. Tian, L. Wang, H. Li, Y. Zhang and X. Sun, *Macromolecules*, 2010, **43**, 10078-10083.
20. P. May, U. Khan, J. M. Hughes and J. N. Coleman, *J. Phys. Chem. C*, 2012, **116**, 11393-11400.
21. J. N. Coleman, *Adv. Funct. Mater.*, 2009, **19**, 3680-3695.
22. U. Khan, P. May, A. O'Neill and J. N. Coleman, *Carbon*, 2010, **48**, 4035-4041.
23. A. O'Neill, U. Khan and J. N. Coleman, *Chem. Mater.*, 2012, **24**, 2414-2421.
24. R. Cooper, H. P. Upadhyaya, T. K. Minton, M. R. Berman, X. Du and S. M. George, *Thin Solid Films*, 2008, **516**, 4036-4039.
25. D. Pacile, J. Meyer, C. O. Girit and A. Zettl, *Appl. Phys. Lett.*, 2008, **92**, 133107-133107-133103.
26. C. Zhi, N. Hanagata, Y. Bando and D. Golberg, *Chemistry–An Asian Journal*, 2011, **6**, 2530-2535.
27. W. Orellana and H. Chacham, *Phys. Rev. B*, 2001, **63**, 125205.
28. N. Jacobson, S. Farmer, A. Moore and H. Sayir, *J. Am. Ceram. Soc.*, 1999, **82**, 393-398.
29. C. G. Cofer and J. Economy, *Carbon*, 1995, **33**, 389-395.
30. K. Simonov, N. A. Vinogradov, M. L. Ng, A. Vinogradov, N. Mårtensson and A. Preobrajenski, *Surf. Sci.*, 2012, **606**, 564-570.
31. M. Petravic, R. Peter, I. Kavre, L. H. Li, Y. Chen, L.-J. Fan and Y.-W. Yang, *Phys. Chem. Chem. Phys.*, 2010, **12**, 15349-15353.
32. Y. Zhao, X. Wu, J. Yang and X. C. Zeng, *Phys. Chem. Chem. Phys.*, 2012, **14**, 5545-5550.
33. X.-H. Zhao, Z.-G. Shen, Y.-S. Xing and S.-L. Ma, *Polym. Degrad. Stabil.*, 2005, **88**, 275-285.
34. J. N. Coleman, M. Lotya, A. O'Neill, S. D. Bergin, P. J. King, U. Khan, K. Young, A. Gaucher, S. De and R. J. Smith, *Science*, 2011, **331**, 568-571.
35. L. Liu, Z. Shen, S. Liang, M. Yi, X. Zhang and S. Ma, *J. Mater. Sci.*, 2014, **49**, 321-328.
36. Y. Shi, C. Hamsen, X. Jia, K. K. Kim, A. Reina, M. Hofmann, A. L. Hsu, K. Zhang, H. Li and Z.-Y. Juang, *Nano Lett.*, 2010, **10**, 4134-4139.
37. P. Nemes-Incze, Z. Osváth, K. Kamarás and L. Biró, *Carbon*, 2008, **46**, 1435-1442.
38. O. Tapasztó, L. Tapasztó, M. Markó, F. Kern, R. Gadow and C. Balázsi, *Chem. Phys. Lett.*, 2011, **511**, 340-343.
39. D. D. Kulkarni, I. Choi, S. S. Singamaneni and V. V. Tsukruk, *ACS nano*, 2010, **4**, 4667-4676.
40. B. Debelak and K. Lafdi, *Carbon*, 2007, **45**, 1727-1734.
41. J. Liang, Y. Huang, L. Zhang, Y. Wang, Y. Ma, T. Guo and Y. Chen, *Adv. Funct. Mater.*, 2009, **19**, 2297-2302.
42. M. A. Rafiee, J. Rafiee, I. Srivastava, Z. Wang, H. Song, Z. Z. Yu and N. Koratkar, *small*, 2010, **6**, 179-183.
43. D. R. Bortz, E. G. Heras and I. Martin-Gullon, *Macromolecules*, 2011, **45**, 238-245.
44. M. K. Shin, B. Lee, S. H. Kim, J. A. Lee, G. M. Spinks, S. Gambhir, G. G. Wallace, M. E. Kozlov, R. H. Baughman and S. J. Kim, *Nat Commun*, 2012, **3**, 650.
45. S. Packirisamy, D. Schwam and M. Litt, *J. Mater. Sci.*, 1995, **30**, 308-320.

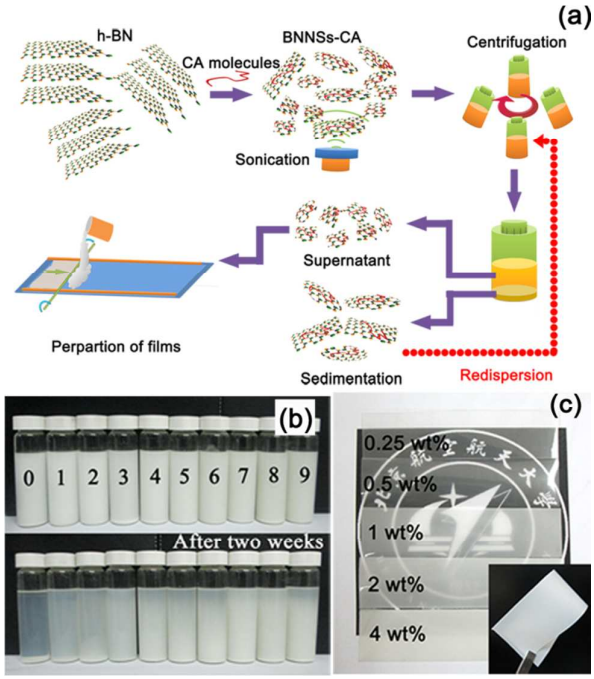

Fig. 1 Schematic illustrations of producing steps of BNNSs/CA composite films (a); Photographs of BNNSs dispersion with different CA concentraions which are 0 - 9 mg ml-1 from left to right, respectively (b); Photograph of pure CA and BNNSs/CA composite films.The inset displays a bent 2 wt% BNNSs/CA composite film (c)

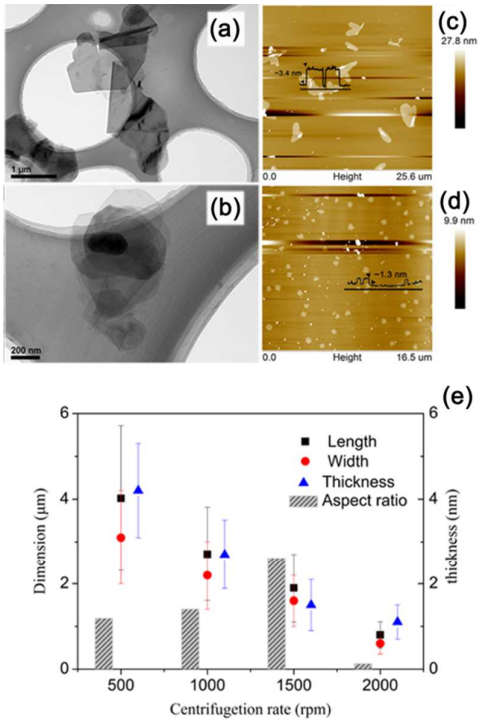

Fig. 2 Representative AFM and TEM images of BNNSs selected with 500 rpm (a, c) and 2000 rpm (b, d); The aspect ratio (length/ thickness), length, width and thickness of BNNSs separated with different final rates (e), and the data points are the average values of 50 measurements

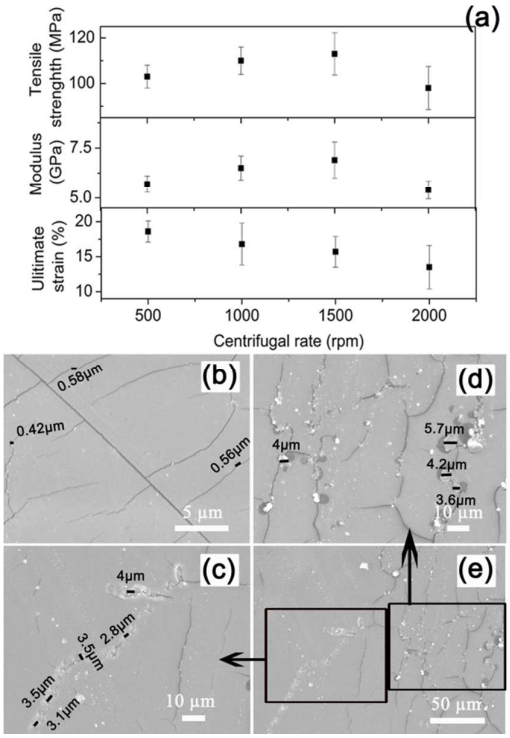

Fig. 3 Young's modulus, tensile strength and uilitmate strain (a) of the pure CA and BNNSs/CA composite films containing 0.5 wt% contents of BNNSs selected with different final speeds; SEM images of cracks in composite films after tensile testing, including 2000 rpm sample (b) and 1000 rpm sample (c-e)

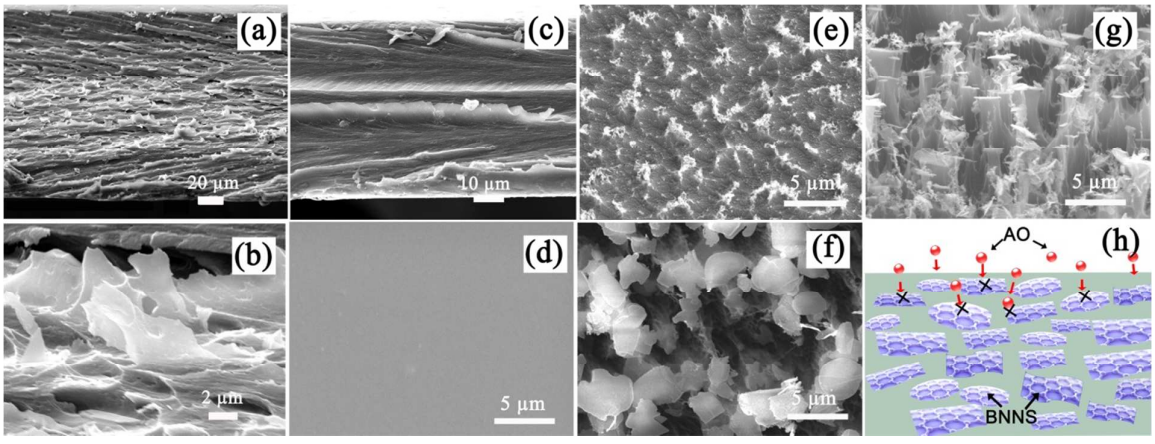

Fig. 4 Representative SEM images of the fractured surfaces of composite films (a,b) and the pure CA film(c) and; Pure CA film before (d) and after (e) AO exposure; The top view (f) and side view (g) of 2 wt% BNNSs/CA composite films after AO exposure; The corrosion protection mechanism of BNNSs (h)

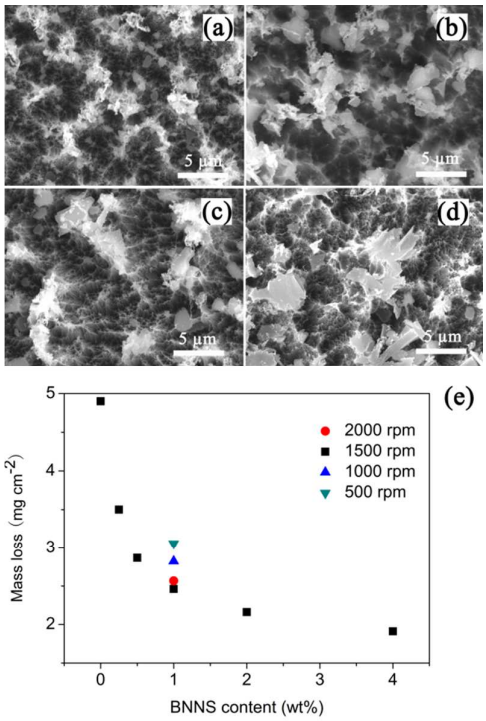

Fig.5 SEM images of 1 wt% BNNSs/CA composite films after AO exposure. BNNSs were separated with final centrifugation rates of 2000 rpm (a), 1500 rpm (b), 1000rpm (c), 500 rpm (d); Mass loss of BNNSs/CA composites after AO exposure (e)

Toc Figure

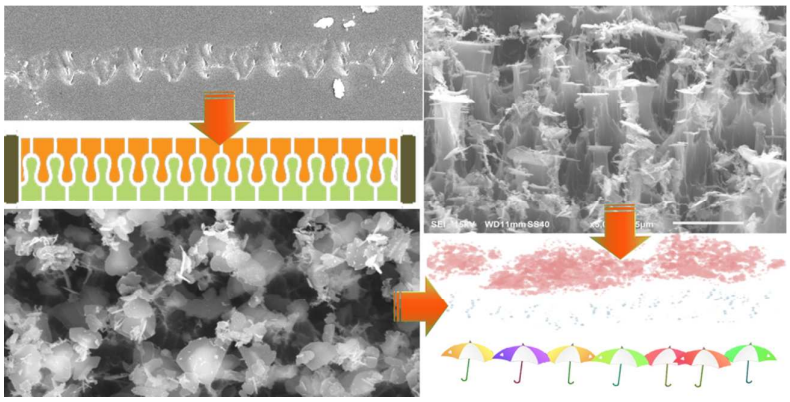

Boron nitride nanosheets exhibited excellent stability and can form three-dimension layered covering to protect underlying polymer from atomic oxygen erosion, and ones of relatively uniform size can promote the formation of "zipper cracks".